sciendo International Journal of Mathematics and Computer in Engineering 3(2) (2025) 201–222

International Journal of Mathematics and Computer in Engineering

https://sciendo.com/journal/IJMCE

Original Study

Thermohaline convection in MHD Casson fluid over an exponentially stretching sheet

Vinod Y.[1], K.R. Raghunatha[1†], Sangamesh[1], Suma Nagendrappa Nagappanavar[1]

[1]Department of Mathematics, Davangere University, Davangere, 577 007, India

Communicated by Haci Mehmet Baskonus; Received: 24.01.2024; Accepted: 06.04.2024; Online: 00.00.2024

Abstract

This study investigates the thermohaline convection in MHD Casson fluid over an exponentially stretching sheet. This study has practical significance in industrial processes, materials processing, energy systems, and environmental applications. The governing equations describing the conservation for an electrically conducting fluid flow, thermal and concentration transports are considered based on the principles of mass, momentum, energy and concentration equations. Our first step involves transforming the governing nonlinear partial differential equations into a coupled nonlinear ordinary differential equations with the help of suitable similarity transformations. Second step, infinite domain $[0, \infty)$ of the problem to a finite domain $[0, 1]$ through a coordinate transformations. This specific choice is motivated by the wavelet's significance in the finite domain of $[0, 1]$. Third step, we effectively solve the resulting coupled nonlinear ordinary differential equations using the numerical Hermite wavelet method (HWM). This approach proves to be a valuable technique for obtaining significant results and insights in our study. Finally, the effect of known physical parameters on velocity, temperature and concentration are analysed through tables and graphs.

Keywords: Boundary layer flow, casson fluid, non-uniform heat source/sink, stretching sheet.
AMS 2020 codes: 34K28; 34K40.

1 Introduction

The flow over a stretching surface is an important problem in many engineering processes with applications in industries such as extrusion, glass-fiber production, the hot rolling, melt-spinning, wire drawing, manufacture of plastic and rubber sheets, cooling of a large metallic plate in a bath, which may be an electrolyte, etc [1, 2]. Experiments show that the velocity of the stretching surface is approximately proportional to the distance from the orifice [3]. Crane [4] studied the steady two-dimensional incompressible boundary layer flow of a Newtonian fluid caused by the stretching sheet. Nazar et al. [5] are studied boundary layer flow in the region of the stagnation point on a stretching sheet. Fang et al. [6] are examined boundary layer flow over a stretching sheet with variable thickness.

In recent years, some interest has been given to the study of convective transport of Non-Newtonian fluids. Non-Newtonian fluids encompass a captivating and diverse group of fluids that present behaviours distinct from the conventional Newtonian fluid model. Diverging from Newtonian fluids, which maintain a consistent viscosity irrespective of the applied shear stress, non-Newtonian fluids possess viscosities that fluctuate in response to external forces. The study of non-Newtonian fluids also has applications in biomedical engineering, geophysics, rheology, and many other fields [7–10]. Casson fluid is one such type of non-Newtonian fluid that is widely

†Corresponding author.
Email address: raghunatha13@davangereuniversity.ac.in

sciendo
ISSN 2956-7068
doi:10.2478/ijmce-2025-0016
sciendo
Open Access.© 2025 Raghunatha et al., published by Sciendo.
This work is licensed under the Creative Commons Attribution alone 4.0 License.

used for modelling blood flow in narrow arteries. Bhattacharyya [11] studied the research examines the stable boundary layer stagnation-point flow and heat transmission of Casson fluid on a sheet undergoing contraction or expansion. Mustafa et al. [12] investigate the time-varying behavior of the flow and heat transfer of a non-Newtonian fluid (Casson fluid) over a moving flat plate that is exposed to a parallel free stream. Stagnation-point flow and heat transfer of a Casson fluid towards a stretching sheet is studied by Mustafa et al. [13]. Mukhopadhyay et al. [14] examined the flow and heat transmission of a Casson past a symmetric wedge, under the forced convection regime.

However, thermohaline convection is a phenomenon that occurs when there are gradients in both temperature and concentration in a fluid. It is a significant topic in fluid mechanics and has several real-life applications [15–17]. Verma and Mondal [18] are reviewed heat and mass transfer of Casson fluids. Ibrahim et al. [19] are investigated how the flow of a non-Newtonian (Casson fluid) is affected by a heat source, suction/injection, and chemical reaction when it passes over an exponentially stretching sheet. Aghighi et al. [20] are examined double-diffusive natural convection of Casson fluids in an enclosure.

Magnetohydrodynamics (MHD) is extensively used as a tool for studying fluid dynamics in general. MHD plays a crucial role in understanding natural phenomena in space propulsion [21], industrial applications [22] and geophysics and astrophysics [23]. It helps in understanding the behavior of conducting fluids in the presence of magnetic fields, including the interaction of magnetic fields with fluid flow [24–26]. Moreover, a non-uniform heat source/sink refers to a situation where the heat generation or absorption within a system is not evenly distributed. This phenomenon has significant implications in various fields, including thermal engineering [27], industrial processes [28] and environmental engineering [29]. The combination of double diffusive convection, non-uniform heat source and magnetic field possesses a wide range of applications [30–32]. A study by Nadeem et al. [33] examined the MHD boundary layer flow of a fluid with Casson rheology over a shrinking sheet that has an exponential permeability.Mukhopadhyay et al. [34] used a computer simulation to study the flow of non- Newtonian (Casson fluid) over a sheet that is stretching exponentially, in the existence of a magnetic flux. Ghilasi and Saleh [35] studied the Casson flow over a stationary plate in the influence of a magnetic flux and a non-uniform heat source/sink using the homotopy analysis method. Bhatti et al. [36] are obtained differential transform solution for Hall and ion-slip effects on radiative-convective Casson flow from a stretching sheet with convective heating. Ganesh and Sridhar [37] are examined the double convection characteristics of a MHD non-Newtonian fluid over an exponentially porous stretching sheet.

Mathematical modeling of various phenomena in diverse fields such as engineering, science and technology often involves nonlinear differential equations. Such nonlinear equations naturally arise in many real-world problems pertaining to fluid dynamics, materials science, physics, biology and other domains [38–40]. However, analytical solutions are rarely feasible for most nonlinear problems except trivial cases. As a result, numerical methods are commonly employed to obtain approximate solutions. In recent years, several numerical techniques have been proposed for solving highly nonlinear differential equations, including the Runge-Kutta method,finite difference approaches, optimal homotopy analysis, homotopy perturbation method, and numerical wavelet approaches. Numerical wavelet methods have gained significant attention in recent years for solving differential equations arising in diverse fields such as signal processing, image analysis and mathematical modeling. Notable contributions include the use of Laguerre wavelets [41], Taylor wavelets [42], cardinal B-splines [43], Bernoulli wavelets [44] and Hermite wavelets [45,46]. Among these, the HWM has been widely utilized due to its accuracy. Given the effectiveness of numerical wavelet techniques, developing a parametric Hermite wavelet approach for nonlinear problems is important. With the availability of powerful computational software, Hermite wavelet methods have been successfully employed by researchers to solve various nonlinear boundary value problems, including different fluid flow models [47–53].

In this paper, we apply the HWM to analyze MHD double diffusive non-Newtonian (Casson fluid) fluid flow of a over a sheet with a variable heat source or sink. Our numerical wavelet results are more effective and accurate than other numerical techniques. The impact of influential physical parameters such as the Prandtl number, Schmidt number, Magnetic field, suction or blowing, chemical reaction and radiation parameters on the velocity, temperature and concentration distributions in the boundary layer are examined.

The paper is organized as follows: Section 2 mathematical model of the problem. Sections 3 and 4 present the methodology of HWM and the integration of matrix, respectively. 5 present the method of solution procedure. Section 6 discusses the results. Section 7 provides the conclusions of this paper.

2 Mathematical model

We examine a steady, laminar boundary layer flow of an incompressible Casson fluid over an exponentially expanding surface aligned with the $y = 0$ plane, with the fluid flow constrained to $y > 0$. This flow increases from the linear stretching of the surface, induced by the concurrent application of two equal and opposite forces along the x-axis. Preserving the original configuration, the sheet stretches at velocity $U_w(x)$. The lower and upper boundaries are held at constant temperatures $T(w)$ and T_∞, respectively, while solute concentration is held at fixed values $C(w)$ and C_∞, respectively, as represented in Figure 1. Within the common boundary layer flow approximations, heat and mass transfer characteristics of the Casson fluid can be described by the following equations for continuity, momentum, energy and concentration in Cartesian coordinates x and y [54, 55]

$$\frac{\partial \mathrm{u}}{\partial \mathrm{x}} + \frac{\partial \mathrm{u}}{\partial \mathrm{y}} = 0, \tag{1}$$

$$u\frac{\partial \mathrm{u}}{\partial \mathrm{x}} + \mathrm{v}\frac{\partial \mathrm{u}}{\partial \mathrm{y}} = \nu\left(1 + \frac{1}{\beta}\right)\frac{\partial^2 \mathrm{u}}{\partial \mathrm{y}^2} - \frac{\sigma B^2 u}{\rho}, \tag{2}$$

$$u\frac{\partial \mathrm{T}}{\partial \mathrm{x}} + \mathrm{v}\frac{\partial \mathrm{T}}{\partial \mathrm{y}} = \frac{\kappa_T}{\rho C_p}\frac{\partial^2 \mathrm{T}}{\partial \mathrm{y}^2} - \frac{1}{\rho C_p}\frac{\partial q_r}{\partial \mathrm{y}} + \frac{Q}{\rho C_p}(T - T_\infty), \tag{3}$$

$$u\frac{\partial \mathrm{C}}{\partial \mathrm{x}} + \mathrm{v}\frac{\partial \mathrm{C}}{\partial \mathrm{y}} = \frac{\kappa_C}{\rho C_p}\frac{\partial^2 \mathrm{C}}{\partial \mathrm{y}^2} - K_1(C - C_\infty), \tag{4}$$

where x- axis velocity (u), y-axis velocity (v), density of fluid (ρ), electrical conductivity (σ), kinematic viscosity(ν), specific heat at constant pressure (C_p), temperature (T), thermal diffusivity (κ_T), dimensional heat source(Q), solute diffusivity (κ_C), chemical reaction(K_1), radiative heat flux (q_r), Casson parameter(β) and magnetic field(B).
Using the Rossel and approximation for radiation, we get

$$q_r = -\frac{4\sigma}{3K^*}\frac{\partial T^4}{\partial y}, T^4 \approx 4T_\infty^3 T - 3T_\infty^4,$$

$$q_r = -\frac{4\sigma}{3K^*}\frac{\partial\left(4T_\infty^3 T - 3T_\infty^4\right)}{\partial y} = -\frac{16\sigma T_\infty^3}{3K^*}\frac{\partial T}{\partial y}. \tag{5}$$

Hence, (3) reduce to

$$u\frac{\partial \mathrm{T}}{\partial \mathrm{x}} + \mathrm{v}\frac{\partial \mathrm{T}}{\partial \mathrm{y}} = \frac{\kappa_T}{\rho C_p}\frac{\partial^2 \mathrm{T}}{\partial \mathrm{y}^2} + \frac{16\sigma T_\infty^3}{3K^*}\frac{1}{\rho C_p}\frac{\partial^2 \mathrm{T}}{\partial \mathrm{y}^2} + \frac{Q}{\rho C_p}(T - T_\infty). \tag{6}$$

The boundary conditions are

$$\begin{aligned} &u = U_w(x),\ \mathrm{v} = -V(x),\ \mathrm{T} = T_w, C = C_w \ \ at \ \ y = 0, \\ &u = 0,\ \mathrm{T} = T_\infty, C = C_\infty \ \ \ at \ \ \ y \to \infty. \end{aligned} \tag{7}$$

The wall and the boundary layer's outer edge have different conditions, which are denoted by the subscripts w and ∞.
Introducing the following similarity variables as

$$\begin{aligned} &\eta = ye^{\frac{x}{2L}}\sqrt{\frac{u_0}{2\nu \mathrm{L}}},\ B = B_0 e^{\frac{x}{2L}},\ \ u = u_0 e^{\frac{x}{L}} f'(\eta),\ \mathrm{v} = -e^{\frac{x}{2L}}\sqrt{\frac{u_0}{2\nu \mathrm{L}}}\left(f(\eta) + \eta f'(\eta)\right) \\ &T = T_\infty + T_0 e^{\frac{x}{2L}}\theta(\eta),\ \ C = C_\infty + C_0 e^{\frac{x}{2L}}\varphi(\eta),\ \ Q = Q_0 e^{\frac{x}{2L}},\ \ K_1 = k_0 e^{\frac{x}{2L}} \end{aligned}. \tag{8}$$

Substitute (8) in (1) to (6) we have,

$$\left(1 + \frac{1}{\beta}\right) f''' + ff'' - 2f'^2 - Mf' = 0, \tag{9}$$

$$\left(1+\frac{4}{3}R\right)\theta''+Pr\left(f\theta'-f'\theta\right)+PrHs\theta=0, \tag{10}$$

$$\varphi''+Sc\left(f\varphi'-f'\varphi\right)-2\gamma\varphi=0. \tag{11}$$

The corresponding boundary conditions becomes,

$$f(0)=S,\ f'(0)=1,\ f'(\infty)\to 0;\theta(0)=1,\theta(\infty)\to 0\,;\varphi(0)=1,\varphi(\infty)\to 0\,. \tag{12}$$

Where, $Pr=\frac{\mu C_p}{\kappa_T}$is the Prandtl number, $M=\frac{\sigma B_0^2 2L}{\mathrm{u}_0\rho}$is the magnetic field parameter, $S=\frac{\mathrm{v}_0}{\sqrt{\frac{u_0 v}{2L}}}$ is the suction or blowing parameter, $Sc=\frac{\mu C_p}{\kappa_C}$is the Schmidt number, $\gamma=\frac{\mathrm{k}_0 L}{\mathrm{u}_0}$is the chemical reaction parameter, $R=\frac{4\sigma T_\infty^3}{\kappa_T K^*}$is the radiation parameter, $Hs=\frac{Q_0}{\rho C_p}\frac{2L}{\mathrm{u}_0\rho}$is the source/sink parameter. Via Table 1, the physical meanings of parameters are given.

Table 1 Nomenclature.

Symbol	Meanings
C_p	Specific heat at constant pressure(J/kg^oC)
B	Magnetic field (Tesla)
C	Concentration of the fluid$\left(mol/m^3\right)$
C_w	Concentration of the wall of the surface$\left(mol/m^3\right)$
C_∞	Free stream concentration
f	Dimensionless stream function
Hs	Heat source/sink parameter
κ_T	Coefficient of thermal diffusivity$\left(m^2/s\right)$
κ_C	Coefficient of solute diffusivity
M	MHD parameter
Pr	Prandtl number
Q^*	Coefficient of heat source $\left(W/m^3\right)$
R	Radiation parameter
S	Suction/blowing parameter
Sc	Schmidt number
T	Temperature of the fluid(K)
T_w	Temperature of the wall of the surface(K)
T_∞	Free stream temperature(K)
u_0	Reference velocity(m/s)
u, v	Velocities in x and y directions (m/s)
x, y	Cartesian coordinates (m)
Greek Symbols	
β	Casson fluid parameter
η	Similarity variable
γ	Chemical reaction parameter
ρ	Density of the fluid$\left(kg/m^3\right)$
ν	Kinematic viscosity $\left(m^2/s\right)$
θ	Non dimensional temperature
φ	Non dimensional concentration

3 Fundamentals of HWM

Hermite wavelets are well-defined as [45, 47],

$$\phi_{n.m}(x)=\begin{cases}\frac{2^{\frac{k-1}{2}}}{\sqrt{\pi}}H_m\left(2^k x-2n+1\right), & \frac{n-1}{2^{k-1}}\le x\le\frac{n}{2^{k-1}}\\ 0 & \text{elsewhere}\end{cases}.$$

Where $n = 1,2,3,\cdots,2^{k-1}$ and $m = 0,1,2,3,\cdots,M-1$ and $k \in N$ Here $H_m(x)$ represents Hermite polynomials of degree m with regards to weight function $W(x) = \sqrt{1-x^2}$ on the real line R and pleases the succeeding recurrence formula $H_0(x) = 1, H_1(x) = 2x, H_{m+2}(x) = 2xH_{m+1}(x) - 2(m+1)H_m(x)$ where, $m = 0,1,2,3,\cdots$.

For a specified nonlinear differential equation, we approximated to the solution as $y(x)$with the assistance of HWM as follows

$$y(x) = \sum_{n=1}^{\infty}\sum_{m=0}^{\infty} C_{n,m}\phi_{n,m}(x).$$

We estimated $y(x)$by truncating the series as follows

$$y(x) \approx \sum_{n=1}^{2^{k-1}}\sum_{m=0}^{M-1} C_{n,m}\phi_{n,m}(x) = A^T\phi(x),$$

where A and $\phi(x)$ are $2^{k-1}M \times 1$ matrix,

$$A^T = [C_{1,0},\cdots C_{1,M-1}, C_{2,0}\cdots C_{2,M-1},\cdots C_{2^{k-1},0},\cdots C_{2^{k-1},M-1}],.$$

$$\phi(x) = [\phi_{1,0},\cdots \phi_{1,M-1}, \phi_{2,0},\cdots \phi_{2,M-1},\cdots \phi_{2^{k-1},0},\cdots \phi_{2^{k-1},M-1}]^T.$$

Let $\{\phi_{i,j}\}$ be the system of Hermite wavelets, n=1, 2, $\cdots$ and m = 0, 1, $\cdots$. For each fixed n, there is a Hermite space generated by the elements of the sequence $\{\phi_{i,j}\}$. That is, $L(\{\phi_{i,j}\}) = H^2[0,1)$ is Banach space.This article is associated to some essential theorems that can be seen in [45, 47].

4 Process of integration of matrix

The following are some of the Hermite wavelet basis at $k = 1$

$$\begin{aligned}
\phi_{1,0}(x) &= \tfrac{2}{\sqrt{\pi}},\\
\phi_{1,1}(x) &= \tfrac{1}{\sqrt{\pi}}(8x-4),\\
\phi_{1,2}(x) &= \tfrac{1}{\sqrt{\pi}}(32x^2-32x+4),\\
\phi_{1,3}(x) &= \tfrac{1}{\sqrt{\pi}}(128x^3-192x^2+48x+8),\\
\phi_{1,4}(x) &= \tfrac{1}{\sqrt{\pi}}(512x^4-1024x^3+384x^2+128x-40),
\end{aligned}$$

$$\phi_{1,5}(x) = \frac{1}{\sqrt{\pi}}(2048x^5-5120x^4+2560x^3+1280x^2-800x+16),$$

$$\phi_{1,6}(x) = \frac{1}{\sqrt{\pi}}(8192x^6-24576x^5+15360x^4+10240x^3-9600x^2+384x+368),$$

$$\phi_{1,7}(x) = \frac{1}{\sqrt{\pi}}(32768x^7-114688x^6+86016x^5+71680x^4-89600x^3+5376x^2+10304x-928),$$

$$\phi_{1,8}(x) = \tfrac{1}{\sqrt{\pi}}(131072x^8-524288x^7+458752x^6+458752x^5-716800x^4+ 57344x^3+164864x^2-29696x-3296),$$

$$\phi_{1,9}(x) = \tfrac{1}{\sqrt{\pi}}(524288x^9-2359296x^8+2359296x^7+2752512x^6-5160960x^5+516096x^4+ 1978368x^3-534528x^2-118656x+21440),$$

$$\phi_{1,10}(x) = \tfrac{1}{\sqrt{\pi}}(2097152x^{10}-10485760x^9+11796480x^8+15728640x^7-34406400x^6+ 4128768x^5+19783680x^4-7127040x^3-2373120x^2+857600x+16448),$$

$$\phi_{1,11}(x) = \tfrac{1}{\sqrt{\pi}}(8388608x^{11}-46137344x^{10}+57671680x^9+86507520x^8-216268800x^7+ 30277632x^6+174096384x^5-78397440x^4-34805760x^3+18867200x^2 +723712x-461696),$$

$$\phi_{1,12}(x) = \frac{1}{\sqrt{\pi}}(33554432x^{12} - 201326592x^{11} + 276824064x^{10} + 461373440x^9 - 1297612800x^8 + 207618048x^7 + 1392771072x^6 - 752615424x^5 - 417669120x^4 + 301875200x^3 + 17369088x^2 - 22161408x + 561536),$$

where, $\phi_9(x) = [\phi_{1,0}(x), \phi_{1,1}(x), \phi_{1,2}(x), \phi_{1,3}(x), \phi_{1,4}(x), \phi_{1,5}(x), \phi_{1,6}(x), \phi_{1,7}(x), \phi_{1,8}(x)]^T$.
Apply the integration regarding with x and limits from 0 to x the above nine bases and explicit it as a linear combination of Hermite wavelet basis as follows.

$$\int_0^x \phi_{1,0}(x) = \left[\tfrac{1}{2}\ \tfrac{1}{4}\ 0\ 0\ 0\ 0\ 0\ 0\ 0\right]\ \phi_9(x),$$

$$\int_0^x \phi_{1,1}(x) = \left[\tfrac{-1}{4}\ 0\ \tfrac{1}{8}\ 0\ 0\ 0\ 0\ 0\ 0\right]\ \phi_9(x),$$

$$\int_0^x \phi_{1,2}(x) = \left[\tfrac{-1}{3}\ 0\ 0\ \tfrac{1}{12}\ 0\ 0\ 0\ 0\ 0\right]\ \phi_9(x),$$

$$\int_0^x \phi_{1,3}(x) = \left[\tfrac{5}{4}\ 0\ 0\ 0\ \tfrac{1}{16}\ 0\ 0\ 0\ 0\right]\ \phi_9(x),$$

$$\int_0^x \phi_{1,4}(x) = \left[\tfrac{-2}{5}\ 0\ 0\ 0\ 0\ \tfrac{1}{20}\ 0\ 0\ 0\right]\ \phi_9(x),$$

$$\int_0^x \phi_{1,5}(x) = \left[\tfrac{-23}{3}\ 0\ 0\ 0\ 0\ 0\ \tfrac{1}{24}\ 0\ 0\right]\ \phi_9(x),$$

$$\int_0^x \phi_{1,6}(x) = \left[\tfrac{116}{7}\ 0\ 0\ 0\ 0\ 0\ 0\ \tfrac{1}{28}\ 0\right]\ \phi_9(x),$$

$$\int_0^x \phi_{1,7}(x) = \left[\tfrac{103}{2}\ 0\ 0\ 0\ 0\ 0\ 0\ 0\ \tfrac{1}{32}\right]\ \phi_9(x),$$

$$\int_0^x \phi_{1,8}(x) = \left[\tfrac{-2680}{9}\ 0\ 0\ 0\ 0\ 0\ 0\ 0\ 0\right]\ \phi_9(x) + \frac{1}{36}\phi_{1,9}(x).$$

Hence,

$$\int_0^x \phi(x)\,dx = H_{9\times 9}\ \phi_9(x) + \bar{\phi}_9(x),$$

where

$$H_{9\times 9} = \begin{bmatrix} \frac{1}{2} & \frac{1}{4} & 0 & 0 & 0 & 0 & 0 & 0 & 0 \\ \frac{-1}{4} & 0 & \frac{1}{8} & 0 & 0 & 0 & 0 & 0 & 0 \\ \frac{-1}{3} & 0 & 0 & \frac{1}{12} & 0 & 0 & 0 & 0 & 0 \\ \frac{5}{4} & 0 & 0 & 0 & \frac{1}{16} & 0 & 0 & 0 & 0 \\ \frac{-2}{5} & 0 & 0 & 0 & 0 & \frac{1}{20} & 0 & 0 & 0 \\ \frac{-23}{3} & 0 & 0 & 0 & 0 & 0 & \frac{1}{24} & 0 & 0 \\ \frac{116}{7} & 0 & 0 & 0 & 0 & 0 & 0 & \frac{1}{28} & 0 \\ \frac{103}{2} & 0 & 0 & 0 & 0 & 0 & 0 & 0 & \frac{1}{32} \\ \frac{-2680}{9} & 0 & 0 & 0 & 0 & 0 & 0 & 0 & 0 \end{bmatrix},\ \overline{\phi_9}(x) = \begin{bmatrix} 0 \\ 0 \\ 0 \\ 0 \\ 0 \\ 0 \\ 0 \\ 0 \\ \frac{1}{36}\phi_{1,9}(x) \end{bmatrix}.$$

Implement the integration to the above nine bases is as follows

$$\int_0^x \int_0^x \phi_{1,0}(x)\,dxdx = \left[\tfrac{3}{16}\ \tfrac{1}{8}\ \tfrac{1}{32}\ 0\ 0\ 0\ 0\ 0\ 0\right]\ \phi_9(x),$$

$$\int_0^x \int_0^x \phi_{1,1}(x)\,dxdx = \left[\tfrac{-1}{6}\ \tfrac{-1}{16}\ 0\ \tfrac{1}{96}\ 0\ 0\ 0\ 0\ 0\right]\ \phi_9(x),$$

$$\int_0^x \int_0^x \phi_{1,2}(x)\,dxdx = \left[\tfrac{-1}{16}\ \tfrac{-1}{12}\ 0\ 0\ \tfrac{1}{192}\ 0\ 0\ 0\ 0\right]\phi_9(x),$$

$$\int_0^x \int_0^x \phi_{1,3}(x)\,dxdx = \left[\tfrac{3}{5}\ \tfrac{5}{16}\ 0\ 0\ 0\ \tfrac{1}{320}\ 0\ 0\ 0\right]\phi_9(x),$$

$$\int_0^x \int_0^x \phi_{1,4}(x)\,dxdx = \left[\tfrac{-7}{12}\ \tfrac{-1}{10}\ 0\ 0\ 0\ 0\ \tfrac{1}{480}\ 0\ 0\right]\phi_9(x),$$

$$\int_0^x \int_0^x \phi_{1,5}(x)\,dxdx = \left[\tfrac{-22}{7}\ \tfrac{-23}{12}\ 0\ 0\ 0\ 0\ 0\ \tfrac{1}{672}\ 0\right]\phi_9(x),$$

$$\int_0^x \int_0^x \phi_{1,6}(x)\,dxdx = \left[\tfrac{81}{8}\ \tfrac{29}{7}\ 0\ 0\ 0\ 0\ 0\ 0\ \tfrac{1}{896}\right]\phi_9(x),$$

$$\int_0^x \int_0^x \phi_{1,7}(x)\,dxdx = \left[\tfrac{148}{9}\ \tfrac{103}{8}\ 0\ 0\ 0\ 0\ 0\ 0\ 0\right]\phi_9(x) + \frac{1}{1152}\phi_{1,9}(x),$$

$$\int_0^x \int_0^x \phi_{1,8}(x)\,dxdx = \left[\tfrac{-773}{5}\ \tfrac{-670}{9}\ 0\ 0\ 0\ 0\ 0\ 0\ 0\right]\phi_9(x) + \frac{1}{1440}\phi_{1,10}(x).$$

Hence,

$$\int_0^x \int_0^x \phi(x)\,dx\,dx = H'_{9\times 9}\,\phi_9(x) + \bar{\phi}'_9(x),$$

where

$$H'_{9\times 9} = \begin{bmatrix} \frac{3}{16} & \frac{1}{8} & \frac{1}{32} & 0 & 0 & 0 & 0 & 0 & 0 \\ \frac{-1}{6} & \frac{-1}{16} & 0 & \frac{1}{96} & 0 & 0 & 0 & 0 & 0 \\ \frac{-1}{16} & \frac{-1}{12} & 0 & 0 & \frac{1}{192} & 0 & 0 & 0 & 0 \\ \frac{3}{5} & \frac{5}{16} & 0 & 0 & 0 & \frac{1}{320} & 0 & 0 & 0 \\ \frac{-7}{12} & \frac{-1}{10} & 0 & 0 & 0 & 0 & \frac{1}{480} & 0 & 0 \\ \frac{-22}{7} & \frac{-23}{12} & 0 & 0 & 0 & 0 & 0 & \frac{1}{672} & 0 \\ \frac{81}{8} & \frac{29}{7} & 0 & 0 & 0 & 0 & 0 & 0 & \frac{1}{896} \\ \frac{148}{9} & \frac{103}{8} & 0 & 0 & 0 & 0 & 0 & 0 & 0 \\ \frac{-773}{5} & \frac{-670}{9} & 0 & 0 & 0 & 0 & 0 & 0 & 0 \end{bmatrix}, \ \overline{\phi'_9}(x) = \begin{bmatrix} 0 \\ 0 \\ 0 \\ 0 \\ 0 \\ 0 \\ 0 \\ \frac{1}{1152}\phi_{1,9}(x) \\ \frac{1}{1440}\phi_{1,10}(x) \end{bmatrix}.$$

Again employ the integration to the above nine bases is as follows

$$\int_0^x \int_0^x \int_0^x \phi_{1,0}(x)\,dxdxdx = \left[\tfrac{5}{96}\ \tfrac{3}{64}\ \tfrac{1}{64}\ \tfrac{1}{384}\ 0\ 0\ 0\ 0\ 0\right]\phi_9(x),$$

$$\int_0^x \int_0^x \int_0^x \phi_{1,1}(x)\,dxdxdx = \left[\tfrac{-7}{128}\ \tfrac{-1}{24}\ \tfrac{-1}{128}\ 0\ \tfrac{1}{1536}\ 0\ 0\ 0\ 0\right]\phi_9(x),$$

$$\int_0^x \int_0^x \int_0^x \phi_{1,2}(x)\,dxdxdx = \left[\tfrac{-1}{80}\ \tfrac{-1}{64}\ \tfrac{-1}{96}\ 0\ 0\ \tfrac{1}{3840}\ 0\ 0\ 0\right]\phi_9(x),$$

$$\int_0^x \int_0^x \int_0^x \phi_{1,3}(x)\,dxdxdx = \left[\tfrac{19}{96}\ \tfrac{3}{20}\ \tfrac{5}{128}\ 0\ 0\ 0\ \tfrac{1}{7680}\ 0\ 0\right]\phi_9(x),$$

$$\int_0^x \int_0^x \int_0^x \phi_{1,4}(x)\,dxdxdx = \left[\tfrac{-13}{56}\ \tfrac{-7}{48}\ \tfrac{-1}{80}\ 0\ 0\ 0\ 0\ \tfrac{1}{13440}\ 0\right]\phi_9(x),$$

$$\int_0^x \int_0^x \int_0^x \phi_{1,5}(x)\,dxdxdx = \left[\tfrac{-65}{64}\ \tfrac{-11}{14}\ \tfrac{-23}{96}\ 0\ 0\ 0\ 0\ 0\ \tfrac{1}{21504}\right]\phi_9(x),$$

$$\int_0^x \int_0^x \int_0^x \phi_{1,6}(x)\,dxdxdx = \left[\tfrac{133}{36}\ \tfrac{81}{32}\ \tfrac{29}{56}\ 0\ 0\ 0\ 0\ 0\ 0\right]\phi_9(x) + \frac{1}{32256}\phi_{1,9}(x),$$

sciendo

$$\int_0^x\int_0^x\int_0^x \phi_{1,7}(x)\,dxdxdx = \left[\tfrac{193}{40}\ \tfrac{37}{9}\ \tfrac{103}{64}\ 0\ 0\ 0\ 0\ 0\ 0\right]\phi_9(x) + \frac{1}{46080}\phi_{1,10}(x),$$

$$\int_0^x\int_0^x\int_0^x \phi_{1,8}(x)\,dxdxdx = \left[\tfrac{-1211}{22}\ \tfrac{-773}{20}\ \tfrac{-335}{36}\ 0\ 0\ 0\ 0\ 0\ 0\right]\phi_9(x) + \frac{1}{63360}\phi_{1,11}(x).$$

Hence,

$$\int_0^x\int_0^x\int_0^x \phi(x)\,dxdxdx = H''_{9\times 9}\,\phi_9(x) + \bar{\phi}''_9(x),$$

where

$$H''_{9\times 9} = \begin{bmatrix} \frac{5}{96} & \frac{3}{64} & \frac{1}{64} & \frac{1}{384} & 0 & 0 & 0 & 0 & 0 \\ \frac{-7}{128} & \frac{-1}{24} & \frac{-1}{128} & 0 & \frac{1}{1536} & 0 & 0 & 0 & 0 \\ \frac{-1}{80} & \frac{-1}{64} & \frac{-1}{96} & 0 & 0 & \frac{1}{3840} & 0 & 0 & 0 \\ \frac{19}{96} & \frac{3}{20} & \frac{5}{128} & 0 & 0 & 0 & \frac{1}{7680} & 0 & 0 \\ \frac{-13}{56} & \frac{-7}{48} & \frac{-1}{80} & 0 & 0 & 0 & 0 & \frac{1}{13440} & 0 \\ \frac{-65}{64} & \frac{-11}{14} & \frac{-23}{96} & 0 & 0 & 0 & 0 & 0 & \frac{1}{21504} \\ \frac{133}{36} & \frac{81}{32} & \frac{29}{56} & 0 & 0 & 0 & 0 & 0 & 0 \\ \frac{193}{40} & \frac{37}{9} & \frac{103}{64} & 0 & 0 & 0 & 0 & 0 & 0 \\ \frac{-1211}{22} & \frac{-773}{20} & \frac{-335}{36} & 0 & 0 & 0 & 0 & 0 & 0 \end{bmatrix}, \overline{\phi''_9}(x) = \begin{bmatrix} 0 \\ 0 \\ 0 \\ 0 \\ 0 \\ 0 \\ \frac{1}{32256}\phi_{1,9}(x) \\ \frac{1}{46080}\phi_{1,10}(x) \\ \frac{1}{63360}\phi_{1,11}(x) \end{bmatrix}.$$

5 Method of solution

The semi-infinite interval in $[0,\infty)$ in (9-11) can be transformed to $[0,1]$ by using the coordinate transformation $\chi = \frac{\eta}{\eta_\infty}$ and the following change of variables

$$F(\chi) = \frac{f(\eta)}{\eta_\infty},\ \ \Theta(\chi) = \frac{\theta(\eta)}{\eta_\infty}, \emptyset(\chi) = \frac{\varphi(\eta)}{\eta_\infty}, \tag{13}$$

where η^∞ is an unknown finite boundary. Using the above transformations, (9-11) becomes

$$\left(1+\frac{1}{\beta}\right)F'''(\chi) + \eta_\infty^2 F(\chi)F''(\chi) - 2\eta_\infty^2 F'^2(\chi) - \eta_\infty^2 MF'(\chi) = 0, \tag{14}$$

$$\left(1+\frac{4}{3}R\right)\Theta''(\chi) + Pr\eta_\infty^2 F(\chi)\Theta'(\chi) - Pr\eta_\infty^2 F'(\chi)\Theta(\chi) + PrHs\eta_\infty^2\Theta(\chi) = 0, \tag{15}$$

$$\emptyset''(\chi) + Sc\eta_\infty^2 F(\chi)\emptyset'(\chi) - Sc\eta_\infty^2 F'(\chi)\emptyset(\chi) - 2\gamma\eta_\infty^2\emptyset(\chi) = 0. \tag{16}$$

The transformed boundary conditions are,

$$F(0) = \frac{S}{\eta_\infty},\ F'(0) = 1, F'(1) = 0;\ \ \Theta(0) = \emptyset(0) = \frac{1}{\eta_\infty},\ \Theta(1) = \emptyset(1) = 0. \tag{17}$$

5.1 The numerical HWM

Let's assume,

$$F'''(\chi) = A^T\phi. \tag{18}$$

Integrate (18), with respect to χ limit varies form 0 toχ, we get,

$$F''(\chi) = F''(0) + A^T\left(H\phi + \bar{\phi}\right). \tag{19}$$

Integrate (19), with respect to χ limit varies form 0 toχ, we get,

$$F'(\chi) = F'(0) + \chi F''0) + A^T\left(H'\phi + \overline{\phi'}\right). \tag{20}$$

Integrate (20), with respect toχlimit varies from 0 toχ, we get,

$$F(\chi) = F(0) + \chi F'(0) + \frac{\chi^2}{2}F''0) + A^T\left(H''\phi + \overline{\phi''}\right), \tag{21}$$

using boundary conditions (17), then the Eqs. (20) and (21) becomes,

$$F(\chi) = \frac{S}{\eta_\infty} + \chi + \frac{\chi^2}{2}F''0) + A^T\left(H''\phi + \overline{\phi''}\right), \tag{22}$$

$$F''(0) = -1 - \left(H'\phi + \overline{\phi'}\right)\big|_{\chi=1}. \tag{23}$$

Again,

$$\Theta''(\chi) = B^T\phi. \tag{24}$$

Integrate (24), with respect toχlimit varies from 0 toχ, we get,

$$\Theta'(\chi) = \Theta'(0) + B^T\left(H\phi + \bar{\phi}\right). \tag{25}$$

Integrate (25), with respect toχlimit varies from 0 toχ, we get,

$$\Theta(\chi) = \Theta(0) + \chi\Theta'(0) + B^T\left(H'\phi + \overline{\phi'}\right), \tag{26}$$

apply boundary conditions (17) then (26) becomes,

$$\Theta'(0) = \frac{-1}{\eta_\infty} - B^T\left(H'\phi + \overline{\phi'}\right)\big|_{\chi=1}. \tag{27}$$

Again,

$$\emptyset''(\chi) = C^T\phi. \tag{28}$$

Integrate (28), with respect toχlimit varies from 0 toχ, we get,

$$\emptyset'(\chi) = \emptyset'(0) + C^T\left(H\phi + \bar{\phi}\right). \tag{29}$$

Integrate (29), with respect toχlimit varies from 0 toχ, we get,

$$\emptyset(\chi) = \emptyset(0) + \chi\emptyset'(0) + C^T\left(H'\phi + \overline{\phi'}\right), \tag{30}$$

apply boundary conditions (17) then (30) becomes,

$$\emptyset'(0) = \frac{-1}{\eta_\infty} - C^T\left(H'\phi + \overline{\phi'}\right)\big|_{\chi=1}. \tag{31}$$

To collocate the equations and obtain the Hermite wavelet's unknown coefficients. We can substitute $F'''(\chi)$, $F''(\chi), F'(\chi)$, $F(\chi), \Theta''(\chi), \Theta'(\chi), \Theta(\chi), \emptyset''(\chi), \emptyset'(\chi), \emptyset(\chi)$ and $F(\chi) = \frac{f(\eta)}{\eta_\infty}$, $\Theta(\chi) = \frac{\theta(\eta)}{\eta_\infty}, \emptyset(\chi) = \frac{\varphi(\eta)}{\eta_\infty}$ in Eqs. (9-11). Utilize collocation steps using$\chi_i = \frac{2i-1}{2N}$, where $i = 1, 2, 3\cdots N$. This step involves selecting suitable values for N based on the problem's requirements. With the collocation points a collection of algebraic equations is formed. The numerical solutions for Eqs. (9-11), subjected to the conditions specified in equation (12), can be obtained using the calculated Hermite wavelet coefficients.

6 Result and discussion

The HWM is applied to study the thermohaline convection in MHD Casson fluid over an exponentially stretching sheet. The heat transfer coefficient $-\theta'(0)$ results obtained from HWM are validated by comparing with other published studies Pramanik [55]. As shown in Table 2, an excellent agreement is observed. This comparison confirms the suitability of HWM over other numerical techniques for solving highly nonlinear coupled differential equations modeling such complex flow problems.

The fluid velocity decreases with increasing stress parameter as shown in Figures 2 and 4. Because, stress is high, the fluid will resist deformation and flow less eagerly. Figure 3 shows that the velocity decreases with increase in the values of the suction/blowing parameter is a result of the interaction between the fluid flow and the applied suction or blowing mechanism. When a suction parameter is applied, it creates a negative pressure gradient in the direction of the flow. This means that the pressure decreases in the direction of the flow. As a result, the fluid is drawn into the system, and the velocity increases. However, as the suction parameter increases beyond a certain point, the negative pressure gradient becomes more significant. This causes a stronger suction effect, leading to a larger draw of fluid into the system. Consequently, the velocity profiles start to decrease because more fluid is being drawn in, reducing the overall velocity within the system. In the case of blowing, a positive pressure gradient is applied in the direction of the flow. This means that the pressure increases in the direction of the flow. Initially, the blowing parameter causes an increase in pressure, which results in an increase in velocity as fluid is pushed through the system. However, as the blowing parameter continues to increase, the positive pressure gradient becomes more substantial. This increased pressure opposes the flow of fluid, leading to a reduction in velocity. The stronger the blowing parameter, the greater the opposition to the fluid flow, causing a decrease in velocity profiles.

In MHD flow, the interaction between the fluid and the magnetic field can lead to changes in the fluid velocity. The specific effect of the magnetic flux on the velocity of the fluid depends on the direction and strength of the magnetic field, as well as the conductivity of the fluid. In general, when the magnetic parameter increases, which typically refers to an increase in the strength of the magnetic field, the velocity of the fluid tends to decrease. This phenomenon is known as magnetohydrodynamic drag force. The decrease in fluid velocity can be attributed to the Lorentz force, which arises due to the interaction between the magnetic field and the moving charged particles in the fluid. The Lorentz force acts perpendicular to both the magnetic field and the direction of fluid flow. As a result, it can oppose the fluid motion and lead to a decrease in velocity. Furthermore, the Lorentz force can also induce fluid currents that circulate in specific patterns, which can further affect the fluid's velocity. These induced currents can create additional resistance to the fluid flow, causing a decrease in velocity as we can observe in Figures 5 and 6.

In the context of temperature profile in Figure 7, increasing the Casson fluid parameter can lead to an increase in the temperature of the fluid. This is because the higher yield stress or plastic viscosity results in a more resistant or sluggish flow behavior. As the fluid requires a greater force to flow, more energy is dissipated as heat due to the increased resistance and interaction between the fluid particles. This dissipated heat can cause a increase in the temperature of the fluid, leading to an increase in the temperature profile. When the suction/blowing parameter increases, it often leads to decreased temperature gradients as shown in Figure 8. In the case of a heat source/sink in a fluid system, the heat added or removed affects the internal energy of the fluid. When the temperature of the fluid increases, it implies that more heat is being added to the system, resulting in an increase in the heat source/sink parameter (Figure 9). The magnetic fluid properties can be influenced by temperature due to the effect of thermal energy on the fluid's molecular structure. When the temperature of a fluid increases seen in Figure 10, the thermal energy causes the molecules within the fluid to move more vigorously, leading to an increase in their kinetic energy. This increased molecular motion can affect the alignment and orientation of the fluid's magnetic dipoles or particles. The temperature profile in a fluid can be influenced by radiative heat transfer. Radiative heat transfer occurs when energy is transferred between objects or regions through electromagnetic waves, without the need for direct physical contact. If there are temperature differences within the fluid, radiation can transfer heat from hotter regions to cooler regions, leading to an increase in the temperature profile (Figure 11). At higher Prandtl numbers, the thermal diffusivity becomes relatively smaller compared to the momentum diffusivity. This means that heat is transported less efficiently compared to momentum in the fluid. Consequently, the convective heat transfer becomes less dominant, and the temperature profiles tend to decrease (Figure 12).

An increasing Schmidt number can lead to a decreasing concentration profile (Figure 13) due to the dom-

inance of momentum transport over mass transport. The enhanced momentum diffusivity allows for more efficient mixing and dispersion of the fluid, which results in a reduction in the concentration gradients. As the chemical reaction parameter increases, the reaction becomes more intense, leading to a more efficient consumption or production of the species involved. This enhanced reaction activity tends to smoothen out concentration gradients and results in a decreasing concentration profile (Figure 14). The Casson fluid and magnetic field parameters effectively reduce the fluid motion, causing the concentration to increase across the boundary layer for improved mass transfer as shown in Figures 15 and 16.

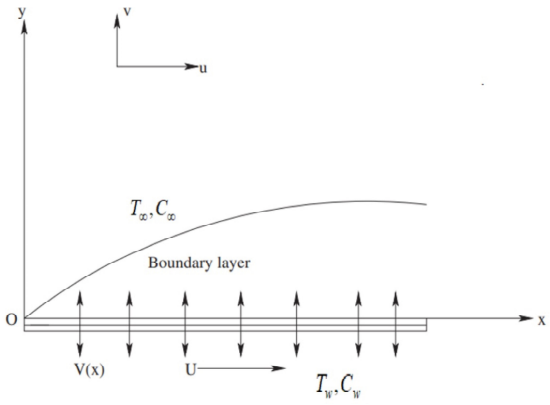

Fig. 1 Physical configuration.

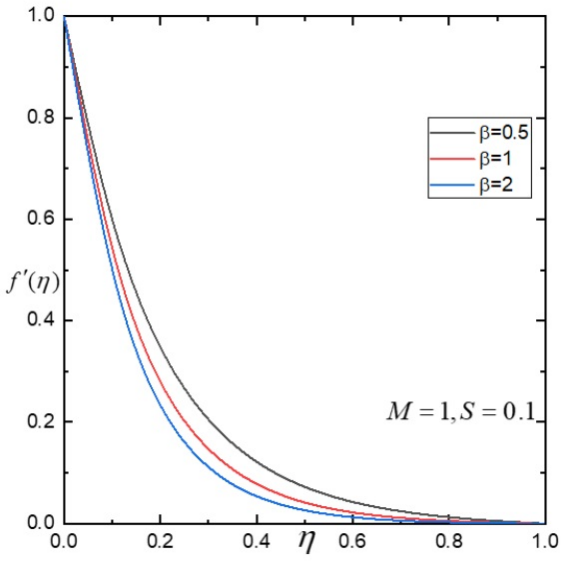

Fig. 2 Influence of β on $f'(\eta)$.

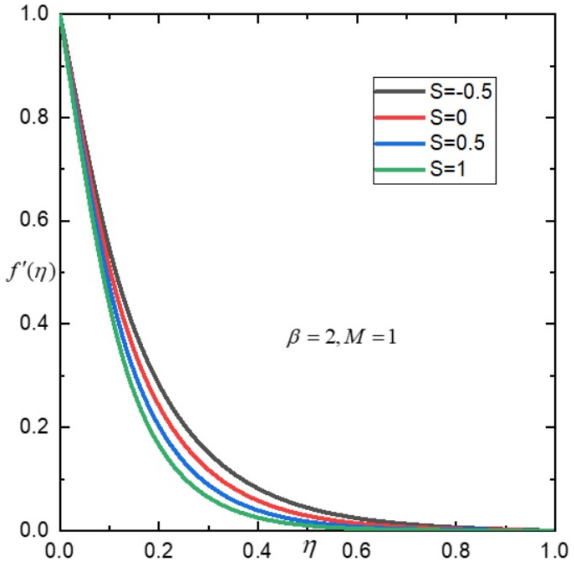

Fig. 3 Influence of S on $f'(\eta)$.

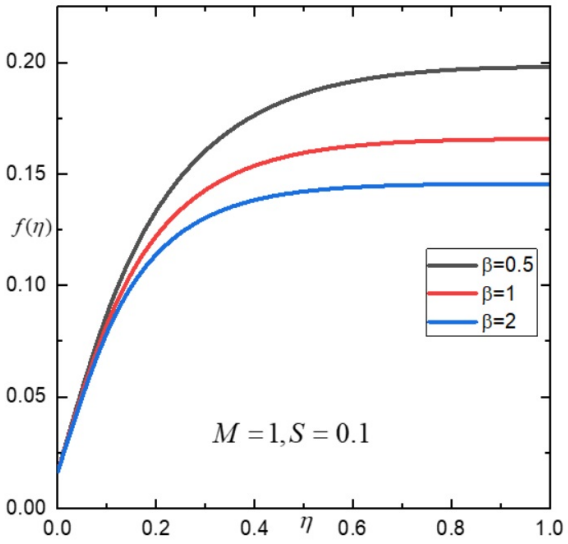

Fig. 4 Influence of β on $f(\eta)$.

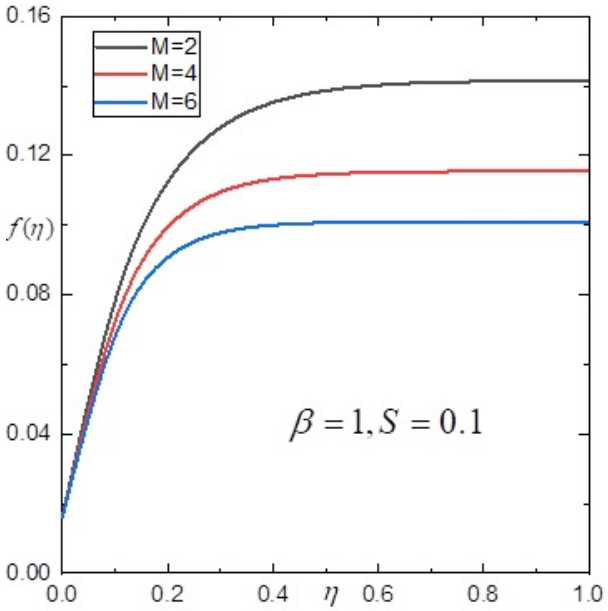

Fig. 5 Influence of M on $f(\eta)$.

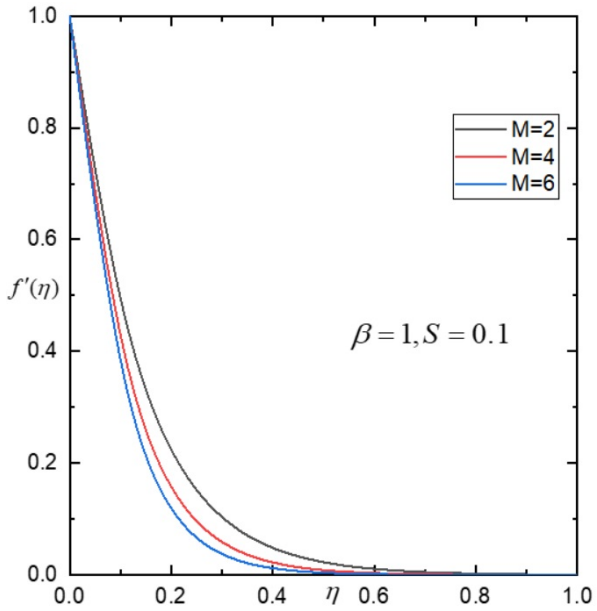

Fig. 6 Influence of M on $f'(\eta)$.

sciendo

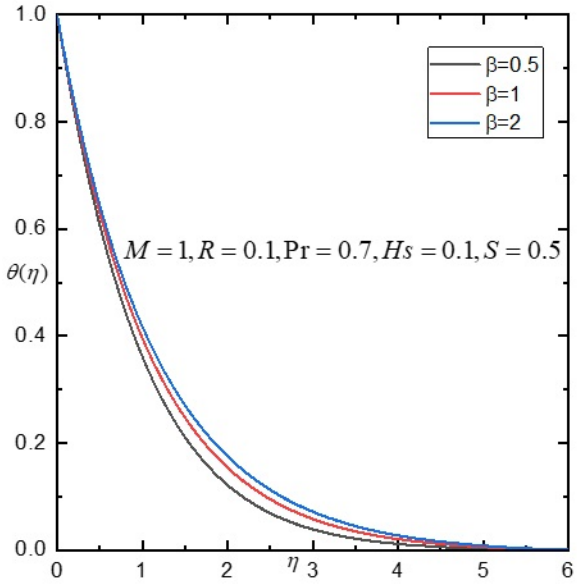

Fig. 7 Influence of β on $\theta(\eta)$.

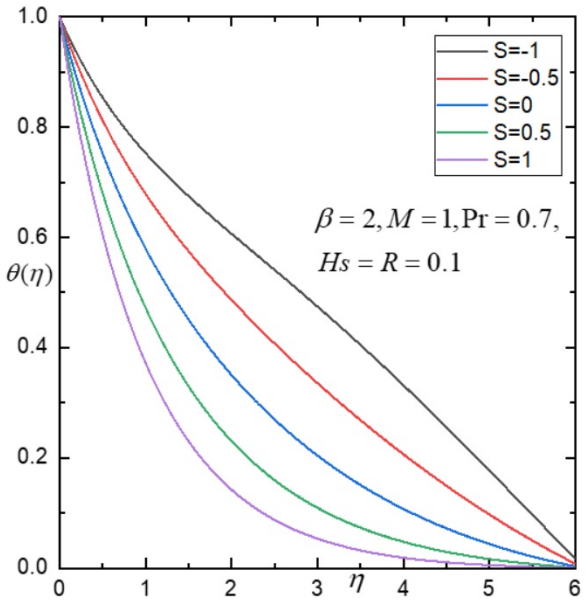

Fig. 8 Influence of S on $\theta(\eta)$.

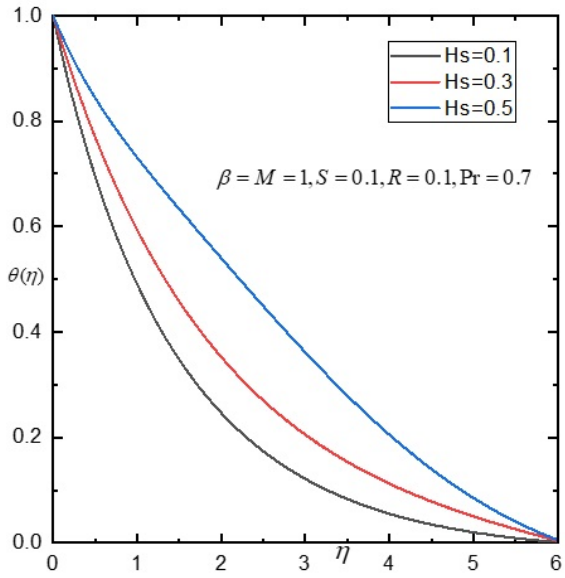

Fig. 9 Influence of Hs on $\theta(\eta)$.

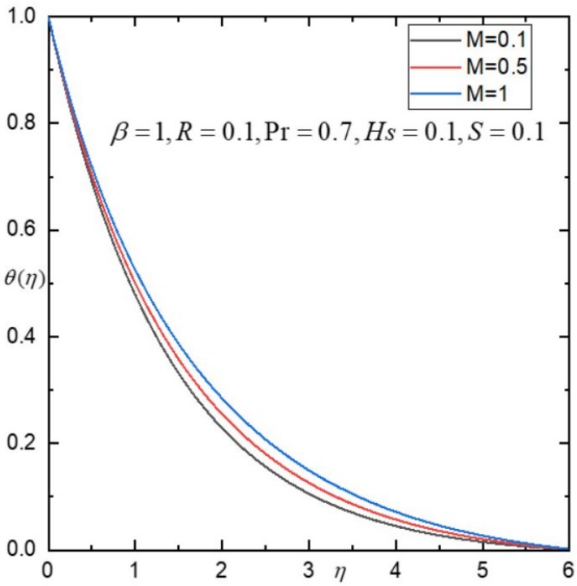

Fig. 10 Influence of M on $\theta(\eta)$.

sciendo

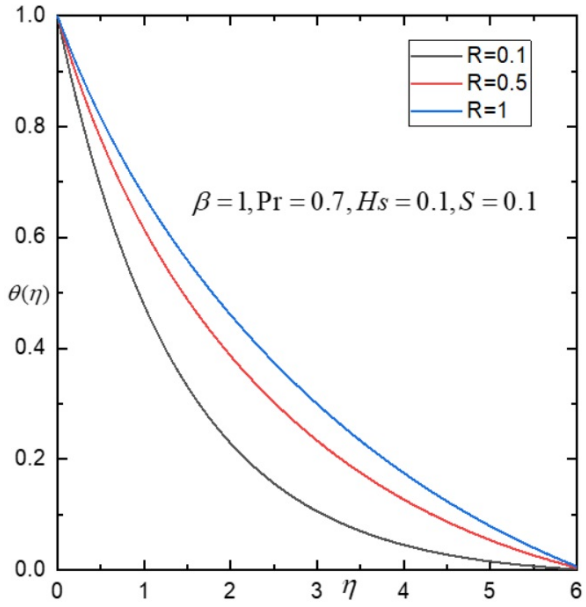

Fig. 11 Influence of R on $\theta(\eta)$.

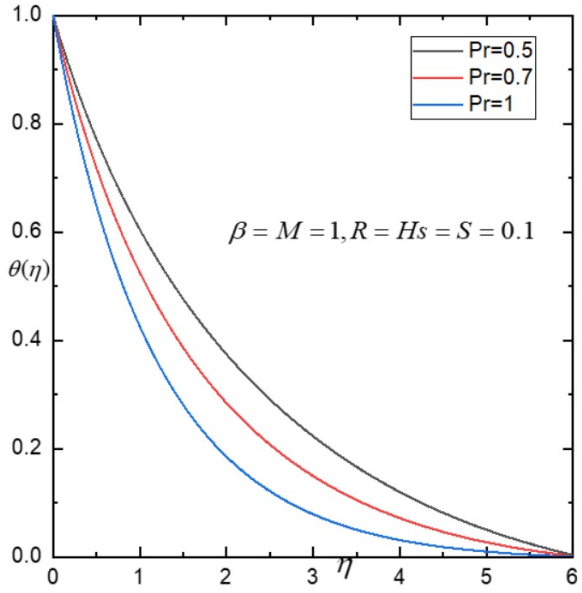

Fig. 12 Influence of Pr on $\theta(\eta)$.

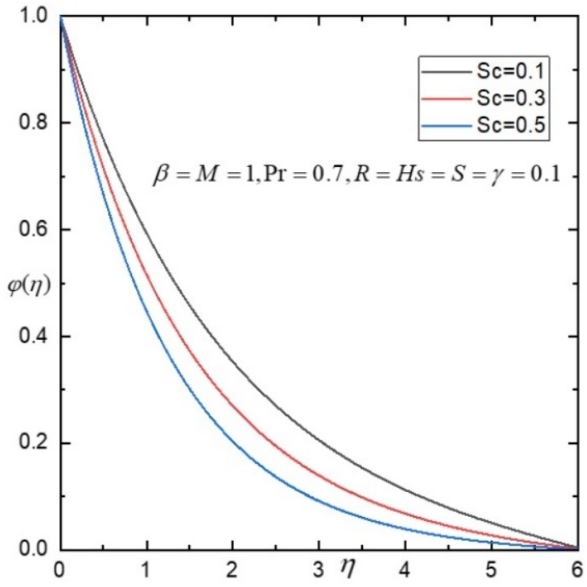

Fig. 13 Influence of *Sc* on $\varphi(\eta)$.

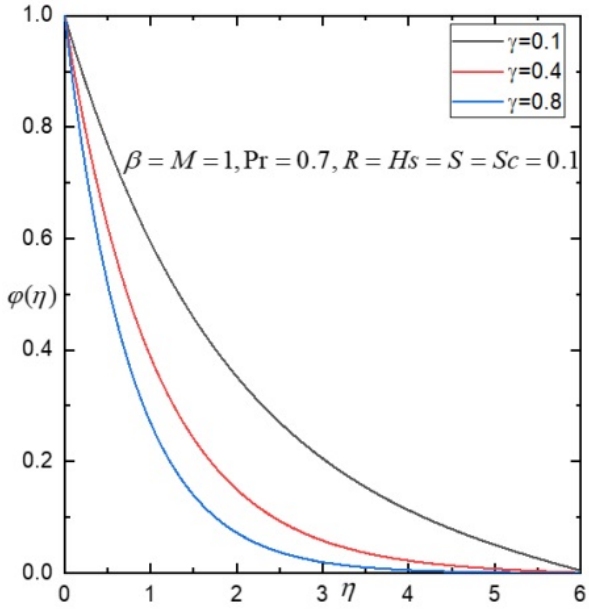

Fig. 14 Influence of γ on $\varphi(\eta)$.

sciendo

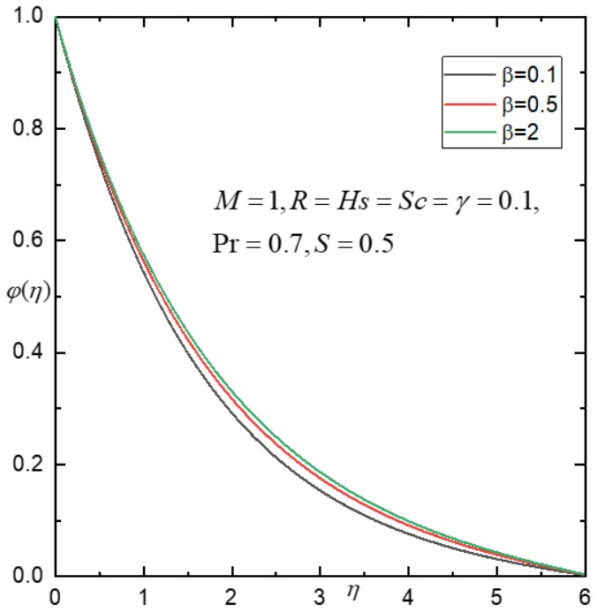

Fig. 15 Influence of β on $\varphi(\eta)$.

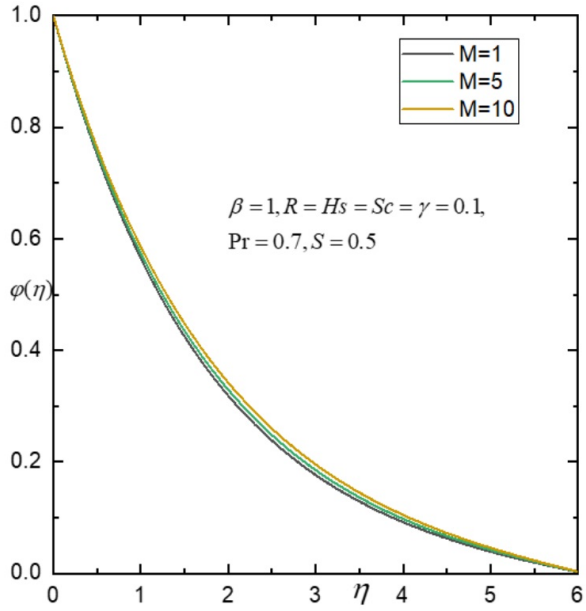

Fig. 16 Influence of M on $\varphi(\eta)$.

Table 2 Comparison of our results with Pramanik [55].

Pr	Bidin and Nazar [56]	HWM with S=M=Hs=Sc=γ=0	Pramanik [55]	Ishak [57]
1	0.9547	0.9547	0.9547	0.9548
2	1.4714	1.4714	1.4714	1.4715
3	1.8691	1.8691	1.8691	1.8691
5	-	2.5001	2.5001	2.5001
10	-	3.6603	3.6603	3.6604

7 Conclusion

The paper applies Hermite wavelet numerical method to solve the governing equations of modeling MHD double diffusive convection in a non-Newtonian fluid (Casson fluid) over an exponentially stretching sheet. The HWM is utilized to handle the highly nonlinear differential equations characterizing the electrically conducting, non-uniform heat source/sink and exponentially stretching sheet problem. We solved the problem by using Mathematica 13.0 version on a 2 G.B. ram sized desktop. Results demonstrated the capability of HWM to accurately solve this complex flow scenario, with solutions closely matching numerical data.

The noteworthy findings obtained from this research can be summarized as follows:

- The fluid velocity decreases with increase in the strength of the magnetic field.
- The temperature of the fluid increases with increasing heat source.
- The temperature profiles decreases with increasing Prandtl number.
- The Schmidt number and chemical reaction parameter are increases leads to a decrease in the concentration gradients of the fluid.

Future work will consider a complex non-Newtonian fluid flow problems analysed in computational fluid dynamics.

8 Declarations

8.1 Conflict of interest:

All the authors declared that there was no conflict of interest.

8.2 Funding:

No funding was received to assist with the preparation of this manuscript.

8.3 Author's Contribution:

V.Y.-Material Preparation, Draft Manuscript, Data Collection and Analysis. K.R.R.-Material Preparation, Draft Manuscript, Data Collection and Analysis. S.N.N.-Material Preparation, Data Collection and Analysis. S.-Material Preparation, Data Collection and Analysis. All authors read and approved the final manuscript.

8.4 Acknowledgement:

The authors wish to thank the reviewers for their useful comments that helped in improving the paper significantly.

8.5 Data availability statement:

All data that support the findings of this study are included within the article.

8.6 Using of AI tools:

The authors declare that they have not used Artificial Intelligence (AI) tools in the creation of this article.

References

[1] Khan W.A., Pop I., Boundary-layer flow of a nanofluid past a stretching sheet, International Journal of Heat and Mass Transfer, 53(11-12), 2477–2483, 2010.
[2] Madhu M., Balaswamy B., Kishan N., Three-dimensional MHD boundary layer flow due to an axisymmetric shrinking sheet with radiation, viscous dissipation and heat source/sink, International Journal of Applied Mechanics and Engineering, 21(2), 393–406, 2016.
[3] Vleggaar J., Laminar boundary-layer behaviour on continuous accelerating surface, Chemical Engineering Science, 32(12), 1517–1525, 1977.
[4] Crane L.J., Flow past a stretching plate, Journal of Applied Mathematics and Physics, 21, 645–647, 1970.
[5] Nazar R., Amin N., Filip D., Pop I., Unsteady boundary layer flow in the region of the stagnation point on a stretching sheet, International Journal of Engineering Science, 42(11-12), 1241–1253, 2004.
[6] Fang T., Zhang J., Zhong Y., Boundary layer flow over a stretching sheet with variable thickness, Applied Mathematics and Computation, 218(13), 7241–7252, 2012.
[7] Lin F.N., Chern S.Y., Laminar boundary-layer flow of non-Newtonian fluid, International Journal of Heat and Mass Transfer, 22(10), 1323-1329, 1979.
[8] Salahuddin T., Awais M., Xia W.F., Variable thermo-physical characteristics of Carreau fluid flow by means of stretchable paraboloid surface with activation energy and heat generation, Case Studies in Thermal Engineering, 25, 100971, 2021.
[9] Salahuddin T., Awais M., A comparative study of Cross and Carreau fluid models having variable fluid characteristics, International Communications in Heat and Mass Transfer, 139, 106431, 2022.
[10] Salahuddin T., Mahmood Z., Khan M., Awais M., A permeable squeezed flow analysis of Maxwell fluid near a sensor surface with radiation and chemical reaction, Chemical Physics, 562, 111627, 2022.
[11] Bhattacharyya K., Boundary layer stagnation-point flow of Casson fluid and heat transfer towards a shrinking/stretching sheet, Frontiers in Heat and Mass Transfer, 4(2), 1–9, 2013.
[12] Mustafa M., Hayat T., Pop I., Aziz A., Unsteady boundary layer flow of a Casson fluid due to an impulsively started moving flat plate, Heat Transfer, 40(6), 563–576, 2011.
[13] Mustafa M., Hayat T., Pop I., Hendi A., Stagnation-point flow and heat transfer of a Casson fluid towards a stretching sheet, Zeitschrift für Naturforschung A, 67(1-2), 70–76, 2012.
[14] Mukhopadhyay S., Mondal I.C., Chamkha A.J., Casson fluid flow and heat transfer past a symmetric wedge, Heat Transfer, 42(8), 665–675, 2013.
[15] Salahuddin T., Javed A., Khan M., Awais M., Bangali H., The impact of Soret and Dufour on permeable flow analysis of Carreau fluid near thermally radiated cylinder, International Communications in Heat and Mass Transfer, 138, 106378, 2022.
[16] Salahuddin T., Khan M., Awais M., A noteworthy impact of heat and mass transpiration near the unsteady rare stagnation region, Pramana, 96(48), 1–8, 2022.
[17] Salahuddin T., Awais M., Khan M., Altanji M., Analysis of transport phenomenon in cross fluid using Cattaneo-Christov theory for heat and mass fluxes with variable viscosity, International Communications in Heat and Mass Transfer, 129, 105664, 2021.
[18] Verma V.K., Mondal S., A brief review of numerical methods for heat and mass transfer of Casson fluids, Partial Differential Equations in Applied Mathematics, 3, 100034, 2021.
[19] Ibrahim S.M., Kumar P.V., Lorenzini G., Analytical modeling of heat and mass transfer of radiative MHD Casson fluid over an exponentially permeable stretching sheet with chemical reaction, Journal of Engineering Thermophysics, 29, 136–155, 2020.
[20] Aghighi M.S., Ammar A., Masoumi H., Double-diffusive natural convection of Casson fluids in an enclosure, International Journal of Mechanical Sciences, 236, 107754, 2022.
[21] Bityurin V.A., Zeigarnik V.A., Kuranov A.L., On a perspective of MHD technology in aerospace applications, 27th Plasma Dynamics and Lasers Conference, New Orleans, USA, 17-20 June 1996.
[22] Marquis D.H., Potential industrial applications of magnetohydrodynamics, IEEE Transactions on Industrial Electronics, 1, 85–90, 1963.
[23] Khater A.H., Moawad S.M., Exact solutions for axisymmetric nonlinear magnetohydrodynamic equilibria of aligned magnetic field and plasma flow with applications to astrophysics and plasma confinement devices, Physics of Plasmas, 16(5), 052504, 2009.
[24] Ghalib M.M., Zafar A.A., Riaz M.B., Hammouch Z., Shabbir K., Analytical approach for the steady MHD conjugate

viscous fluid flow in a porous medium with nonsingular fractional derivative, Physica A: Statistical Mechanics and its Applications, 554, 123941, 2020.
[25] Shafiq A., Hammouch Z., Oztop H.F., Radiative MHD flow of third-grade fluid towards a stretched cylinder, 4th International Conference on Computational Mathematics and Engineering Sciences (CMES-2019), Springer, 4, 166–185, 2020.
[26] Zafar A.A., Riaz M.B., Hammouch Z., A class of exact solutions for unsteady MHD natural convection flow of a viscous fluid over a moving inclined plate with exponential heating, constant concentration and chemical reaction, 4th International Conference on Computational Mathematics and Engineering Sciences (CMES-2019), Springer, 4, 218–232, 2020.
[27] Sajid T., Jamshed W., Eid M.R., Algarni S., Alqahtani T., Ibrahim R.W., Ishad K., Hussain S.M., Din S.M.E., Thermal case examination of inconstant heat source (sink) on viscous radiative Sutterby nanofluid flowing via a penetrable rotative cone, Case Studies in Thermal Engineering, 48, 103102, 2023.
[28] Ramesh G.K., Shehzad S.A., Rauf A., Chamkha A.J., Heat transport analysis of aluminum alloy and magnetite graphene oxide through permeable cylinder with heat source/sink, Physica Scripta, 95(8), 095203, 2020.
[29] Chen L., Fu B., Zhao W., Source-sink landscape theory and its ecological significance, Frontiers of Biology in China, 3, 131–136, 2008.
[30] Mondal S., Sibanda P., Unsteady double diffusive convection in an inclined rectangular lid-driven enclosure with different magnetic field angles and non-uniform boundary conditions, International Journal of Heat and Mass Transfer, 90, 900–910, 2015.
[31] Manjula S.H., Suresh P., Rao M.G., The effect of thermal modulation on double diffusive convection in the presence of applied magnetic field and internal heat source, International Journal of Applied Mechanics and Engineering, 26(1), 135–155, 2020.
[32] Mohammadi M., Nassab S.A.G., Bifurcation analysis of combined double diffusive natural convection and thermal radiation under a non-uniform magnetic field in a wavy enclosure, Thermal Science and Engineering Progress, 46, 102192, 2023.
[33] Nadeem S., Haq R.U., Lee C., MHD flow of a Casson fluid over an exponentially shrinking sheet, Scientia Iranica, 19(6), 1550–1553, 2012.
[34] Mukhopadhyay S., Moindal I.C., Hayat T., MHD boundary layer flow of Casson fluid passing through an exponentially stretching permeable surface with thermal radiation, Chinese Physics B, 23(10), 104701, 2014.
[35] Ghiasi E.K., Saleh R., 2D flow of Casson fluid with non-uniform heat source/sink and Joule heating, Frontiers in Heat and Mass Transfer, 12(4), 1–7, 2019.
[36] Bhatti M.M., Khan S.U., Bég O.A., Kadir A., Differential transform solution for Hall and ion-slip effects on radiative-convective Casson flow from a stretching sheet with convective heating, Heat Transfer, 49(2), 872–888, 2020.
[37] Ganesh G.R., Sridhar W., Numerical approach of heat and mass transfer of MHD Casson fluid under radiation over an exponentially permeable stretching sheet with chemical reaction and hall effect, Frontiers in Heat and Mass Transfer, 16(1), 1–11, 2021.
[38] Schulz M., Control Theory in Physics and Other Fields of Science: Concepts, Tools, and Applications, Springer, 2006.
[39] Ivancevic V.G., Ivancevic T.T., Applied Differential Geometry: A Modern Introduction, World Scientific, 2007.
[40] Sun H., Zhang Y., Baleanu D., Chen W., Chen Y.Q., A new collection of real world applications of fractional calculus in science and engineering, Communications in Nonlinear Science and Numerical Simulation, 64, 213–231, 2018.
[41] Shiralashetti S.C., Kumbinarasaiah S., Laguerre wavelets collocation method for the numerical solution of the Benjamina-Bona-Mohany equations, Journal of Taibah University for Science, 13(1), 9–15, 2019.
[42] Shiralashetti S.C., Hanaji S.I., Taylor wavelet collocation method for Benjamin-Bona-Mahony partial differential equations, Results in Applied Mathematics, 9, 100139, 2021.
[43] Shiralashetti S.C., Kumbinarasaiah S., Cardinal B-spline wavelet based numerical method for the solution of generalized Burgers-Huxley equation, International Journal of Applied and Computational Mathematics, 4(73), 1-13, 2018.
[44] Raghunatha K.R., Vinod Y., Nagappanavar S.N., Sangamesh, Unsteady Casson fluid flow on MHD with an internal heat source, Journal of Taibah University for Science, 17(1), 2271691, 2023.
[45] Shiralashetti S.C., Kumbinarasaiah S., Hermite wavelets operational matrix of integration for the numerical solution of nonlinear singular initial value problems, Alexandria Engineering Journal, 57(4), 2591–2600, 2018.
[46] Raghunatha K.R., Vinod Y., Manjunatha B.V., Application of Bernoulli wavelet method on triple-diffusive convection in Jeffery-Hamel flow, Heat Transfer, 52(8), 5269–5301, 2023.
[47] Kumbinarasaiah S., Raghunatha K.R., The applications of Hermite wavelet method to nonlinear differential equations arising in heat transfer, International Journal of Thermofluids, 9, 100066, 2021.
[48] Raghunatha K.R., Vinod Y., Viscous flow by expanding or shrinking the gap with permeable walls through Hermite wavelet method, International Journal of Applied and Computational Mathematics, 9(22), 1–15, 2023.
[49] Kumbinarasaiah S., Raghunatha K.R., Rezazadeh M., Inc M., A solution of coupled nonlinear differential equations arising in a rotating micropolar nanofluid flow system by Hermite wavelet technique, Engineering with Computers, 38, 3351–3372, 2022.

[50] Kumbinarasaiah S., Raghunatha K.R., Numerical solution of the Jeffery-Hamel flow through the wavelet technique, Heat Transfer, 51(2), 1568–1584, 2022.
[51] Raghunatha K.R., Kumbinarasaiah S., Application of Hermite wavelet method and differential transformation method for nonlinear temperature distribution in a rectangular moving porous fin, International Journal of Applied and Computational Mathematics, 8(25), 1–20, 2022.
[52] Faheem M., Khan A., Raza A., A high-resolution Hermite wavelet technique for solving space-time-fractional partial differential equations, Mathematics and Computers in Simulation, 194, 588–609, 2022.
[53] Vinod Y., Raghunatha K.R., Application of Hermite wavelet method for heat transfer in a porous media, Heat Transfer, 52(1), 983–999, 2023.
[54] Swain I., Mishra S.R., Pattanayak H.B., Flow over exponentially stretching sheet through porous medium with heat source/sink, Journal of Engineering, 2015(ID:452592), 1–7, 2015.
[55] Pramanik S., Casson fluid flow and heat transfer past an exponentially porous stretching surface in presence of thermal radiation, Ain Shams Engineering Journal, 5(1), 205–212, 2014.
[56] Bidin B., Nazar R., Numerical solution of the boundary layer flow over an exponentially stretching sheet with thermal radiation, European Journal of Scientific Research, 33(4), 710–717, 2009.
[57] Ishak A., MHD boundary layer flow due to an exponentially stretching sheet with radiation effect, Sains Malaysiana, 40(4), 391–395, 2011.